processes

MDPI

Article

A Numerical Study on the Flow Mechanism of Performance Improvement of a Wide-Angle Diffuser by Inserting a Short Splitter Vane

Xu Meng [1], Zhigang Zuo [1,*], Michihiro Nishi [2], and Shuhong Liu [1,*]

[1] State Key Laboratory of Hydro Science and Engineering, Department of Energy and Power Engineering, Tsinghua University, Beijing 100084, China; zgbh.mx@163.com

[2] Senior Academy, Kyushu Institute of Technology, Tobata 804-8550, Kitakyushu, Japan; nishi.michihiro@gmail.com

* Correspondence: zhigang200@mail.tsinghua.edu.cn (Z.Z.); liushuhong@mail.tsinghua.edu.cn (S.L.); Tel.:+86-10-62773947 (Z.Z. and S.L.)

Received: 25 December 2019; Accepted: 19 January 2020; Published: 22 January 2020

Abstract: Usage of a wide-angle diffuser may result in unfavorable separated flow and a significant diffuser loss. To improve the performance of the diffusers, inserting short splitter vanes is known as a useful method that has been demonstrated experimentally. Regarding the role of the vane in the diffuser flow, Senoo & Nishi (1977) qualitatively explained that the lift force acting on the vane should be a key factor. However, its quantitative verification remains since then. To challenge this issue, numerical simulations of incompressible flow in a wide angle of 28° two-dimensional diffuser with and without a short splitter vane were conducted in the present study. An improvement of pressure-recovery by the vane and oscillatory flows in the diffuser are reasonably reproduced from comparison with the experimental results made by Cochran & Kline (1958). It is also found that the lift force acting on the vane varies periodically in an opposite phase with the detachment point moved back and forth on a diverging wall, since one vane is not sufficient to fully suppress the flow separation that occurred on the wall and the incoming main-flow shifts toward the other diverging wall in the diffuser. Thus, as a role of splitter vane in the diffuser, "the lift force of the vane is a key factor" may be quantitatively verified from the present numerical simulation. Further, it is confirmed by the local loss analysis that the turbulent kinetic energy production observed in mixing layers contributes most of the loss in the diffuser. Consequently, the present numerical technique may be usable to investigate the flow character in a diffuser with splitter vanes at a design stage.

Keywords: wide-angle diffuser; splitter vane; flow simulation; loss analysis; flow mechanism

1. Introduction

Diffusers are widely used in fluid machines and model test facilities (e.g., draft tubes of turbines [1–3], subsonic wind tunnels [4,5], etc. [6]) as a component to convert the dynamic pressure to the static pressure by decelerating the main flow velocity. If the diffuser loss Δp_{Loss} is required to design the above-mentioned systems, the following relationships derived from the one-dimensional theory for the incompressible steady flow have been used [7–9]:

$$\zeta_d \left(= \frac{\Delta p_{Loss}}{q_1} \right) = C_{p_i} - C_p = C_{p_i} \left(1 - \frac{C_p}{C_{pi}} \right) = C_{p_i} \left(1 - \eta_d \right) \quad (1)$$

$$C_{p_i} = 1 - \left(\frac{A_1}{A_2} \right)^2 = 1 - \left(\frac{1}{A_R} \right)^2 \quad (2)$$

$$C_p = \frac{p_2 - p_1}{q_1} \tag{3}$$

$$q_1 = \frac{1}{2}\rho V_1^2 \tag{4}$$

where ζ_d, Cp_i, Cp, and η_d are the diffuser loss coefficient, the ideal and the actual static-pressure recovery coefficients, and the diffuser effectiveness, respectively. And A_R denotes the area-ratio of the diffuser exit area A_2 to the inlet A_1. p_1, p_2, q_1, V_1, and ρ are the inlet and the exit static pressures [Pa], the dynamic pressure at the diffuser inlet [Pa], inlet velocity [m/s] and fluid density [kg/m^3], respectively.

It is known that the diffuser performances given by ζ_d and Cp primarily depend on Reynolds number, inflow conditions (i.e., velocity distribution, main-flow turbulence), and diffuser geometries (i.e., divergence angle, area-ratio, and diffuser length) [8]. Taking into account those parameters mentioned above, extensive studies have been conducted experimentally to prepare selection charts of diffuser geometries associated with pressure recovery and flow characteristics as a convenient tool to design two-dimensional [9], conical [10] and annular diffusers [11].

According to the selection chart (or performance map), diffusers with the divergence angle around 7° may have favorable geometry of duct to provide a low loss, a high pressure-recovery and a stable flow. In some cases of application, however, much wider divergence-angles have to be selected due to the limitation of the axial diffuser length for a given area-ratio. Owing to this selection, the adverse pressure gradient becomes steeper along the diffuser wall, and separation of flow may occur in the diffuser. Once the flow-separation (or stall) takes place in a diffuser, unsteadiness, and non-uniformity of flow are apt to appear at the diffuser exit, and the diffuser loss usually increases together with the decrease of pressure recovery. Thus, many investigations have been carried out to develop separation-control methods including boundary layer suction [12], jet injection [13], high-level turbulence at the inlet [14], passive and active vortex generators [15–17], installation of splitter vanes [7,8,18–20], etc. [21]. Note that Sun et al. [22] performed a numerical investigation of the flow rectification of a vaned micro diffuser.

Historically, flow in a diffuser near the stall condition had been treated almost experimentally because the prediction of separation point was hard to achieve from Prandtl's boundary layer analysis, where the interaction between the boundary layer and the adjacent free-stream wasn't considered [23,24]. Furthermore, a fundamental issue from the viewpoint of fluid mechanics was presented by the results from a wide-angle diffuser with splitter vanes [25]. That is, why is the separating flow suppressed by inserting short splitter vanes into the inlet region of a wide-angle diffuser? Though Senoo and Nishi [26] qualitatively explained that the lift force acting on the vane should be a key factor, its quantitative verification still remains to be done.

In order to challenge the unresolved issue mentioned above, numerical simulation of incompressible flow in a wide-angle two-dimensional diffuser with and without a short splitter vane is conducted in this study.

2. Methodology

2.1. Test Diffuser and Pressure Recovery

In the present study, a specific wide-angle diffuser with and without a splitter vane was investigated. As a test straight diffuser for numerical simulation, we reproduced the geometry used by Cochran and Kline [7]. Referring to their experimental results obtained at the throat Reynolds number of 2.4×10^5, the divergence angle of 28° and the area-ratio of 4.9 were chosen. Thus, the mean velocity at the diffuser throat is 47.85 m/s in the present cases.

The following pressure recovery coefficient C_{PR} is used to evaluate the diffuser performance in the present simulation for direct comparison with the experimental values:

$$C_{PR} = \frac{\frac{1}{A_2}\int_{A_2} p_2 dA_2 - \frac{1}{A_1}\int_{A_1} p_1 dA_1}{\frac{1}{A_1}\int_{A_1} q_1 dA_1} \quad (5)$$

2.2. Numerical Technique

Figure 1 shows the top view of the computational domain, and its depth is 611 mm. As shown in the figure, upstream and downstream channels are added to the domain to take account for the boundary conditions. Specifically, the upstream channel is 1.5 times the length of its width (width of the upstream channel = $8W_1$), and the downstream-channel [5] is 3 times the length of its width (width of the downstream channel = $16W_1$), where W_1 denotes the throat width.

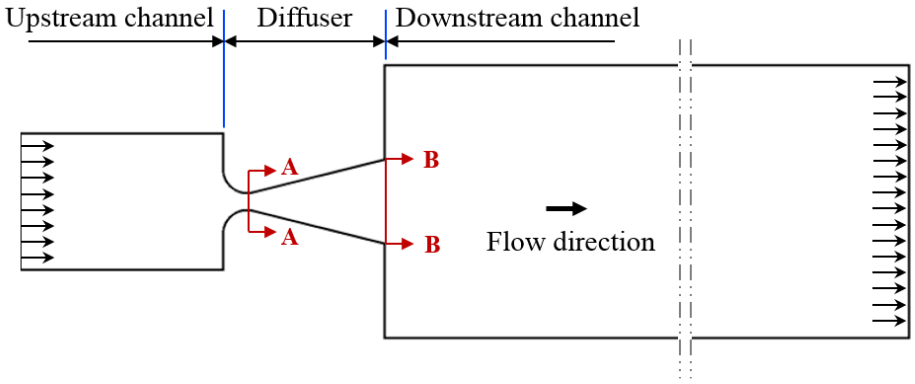

Figure 1. Top view of the computational domain.

Ideal dry air (20 °C) was used as the working fluid. Its uniform velocity at the inlet of the upstream channel and atmospheric pressure at the outlet of the downstream channel were chosen as the boundary conditions. According to the Reynolds number at the diffuser throat mentioned before, the mean velocity was set as 5.96 m/s at the inlet of the upstream channel. The specification method of "Intensity and Viscosity Ratio" was chosen. The turbulence intensity is 5% and the turbulent viscosity ratio is 10. "No-slip" conditions were imposed on all stationary walls. Figure 2 shows the geometrical parameters of the diffuser with and without a short splitter vane (or flat vane), whose major dimensions are listed in Table 1, where it is seen that the numerical test has only one vane length, which is nearly a quarter of the diffuser length. Note that all wall surfaces were smooth following the experiment [7].

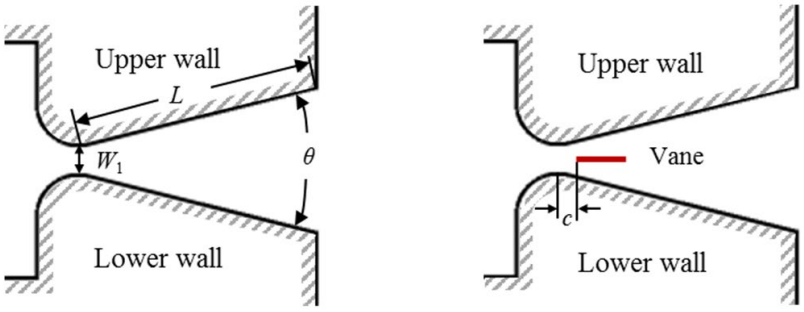

(**a**) Unvaned diffuser (**b**) Vaned diffuser

Figure 2. Geometries of test diffusers.

Table 1. Major dimensions of test diffuser and vane.

	Symbol	Nomenclature	Value
Diffuser	θ (°)	divergence angle	28
	W_1 (mm)	throat width	76
	L/W_1	dimensionless diffuser wall length	8
Vane	L_v (mm)	length	152.4
	δ (mm)	thickness	2.8
	c (mm)	location	44

To study the boundary layer and the large separated flow in the diffuser before and after inserting the splitter vane, a low-Reynolds-number RANS (Reynolds Averaged Navier-Stokes) turbulence model, i.e., SST k-ω turbulence model was applied to this double precision simulation, where wall function was not used. It has been shown that SST k-ω has good compatibility in simulating flow separations [27,28]. SIMPLEC (Semi-Implicit Method for Pressure-Linked Equations Consistent) algorithm with a second-order spatial discretization and a first-order implicit transient formulation were chosen as the pressure-velocity coupling method.

Structured grid-systems for the whole calculation domain were developed by using commercial software ICEM-CFD (Integrated Computer Engineering and Manufacturing code for Computational Fluid Dynamics) in this study. Figure 3 shows the calculation grids. Figure 3a is the local grid refinements near the edge of the diffuser throat and Figure 3b is the top view of the topology of the mesh. To ensure that the first boundary grid layer is located in a viscous sublayer, required by the SST k-ω turbulence model, local grid refinements to the boundary layers were applied at the vane and diffuser walls. Figure 4 shows y^+ distributions on the diverging walls obtained at steady flow simulation of the diffuser without a vane (or unvaned diffuser). "Ideally, while using enhanced wall treatment, the wall y^+ should be in the order of 1 (at least less than 5) to resolve the viscous sublayer" [29]. In our simulations, it is controlled less than 5.

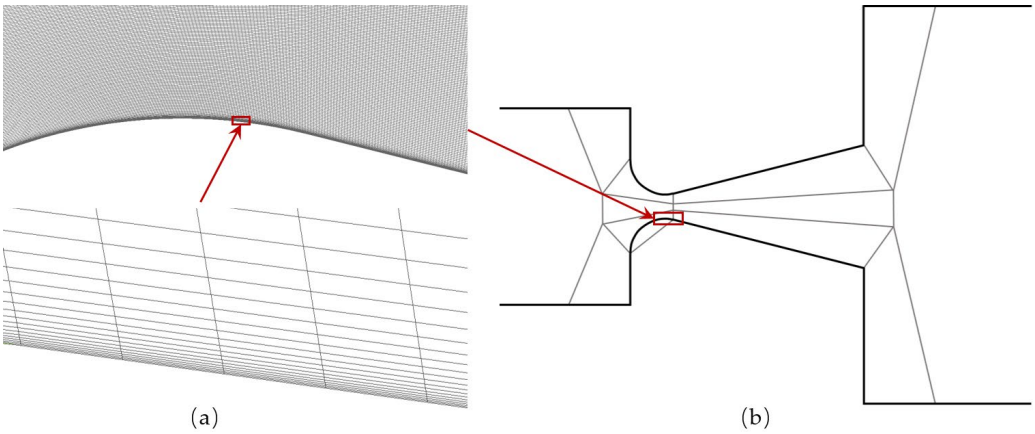

Figure 3. Calculation grids. (**a**) Local grid refinements near the edge of the diffuser throat; (**b**) Topology of the mesh.

Unsteady numerical simulations also based on RANS method were applied in the present study. Considering the grid-scale and the Courant number requirement, i.e., $C = u\Delta t/\Delta s < 10$ (where u, Δt, and Δs are the characteristic flow velocity, the time step size and typical cell size, respectively), Δt was set as 0.001 s. The maximum number of iterations was set as 20. Simulation convergence was achieved when the residual error was lower than 10^{-6}, or the variation of the operational parameter C_{PR} was below 0.01%. For the purpose of measuring the operational parameter C_{PR}, static pressure monitors were set to record the average static pressure of the diffuser inlet and outlet.

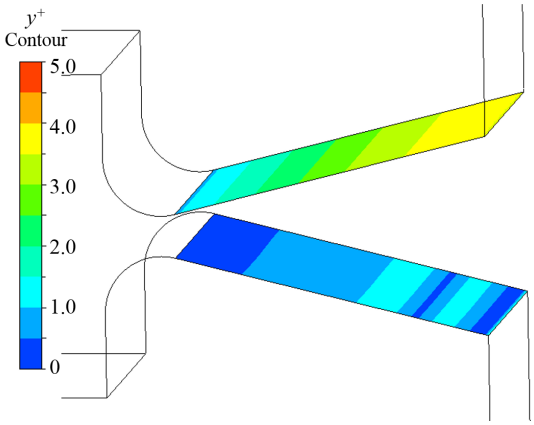

Figure 4. Distributions of y^+ on the diffuser walls.

As preliminary tests, predicted C_{PR} of steady flow simulations by using five mesh systems for both unvaned and vaned diffusers were carried out to find the plausible number of grids for the computational domain. The corresponding results are shown in Figure 5 and the mesh sensitivity analysis is summarized in Table 2, where the following features are observed: C_{PR} becomes almost constant in the region of the number of grids greater than 4.2×10^5 for the unvaned diffuser and 5.9×10^5 for the vaned diffuser. In Table 2, relative change in C_{PR} given by the following expression is used to evaluate the mesh sensitivity. Note that i (2~5) is the serial number of the grid.

$$\frac{\left|C_{PR}(i)-C_{PR}(i-1)\right|}{C_{PR}(i-1)}\times 100\%$$

Therefore, the mesh system with an 8.3×10^5 grid for the unvaned diffuser and that with a 9.7×10^5 grid for the vaned diffuser were chosen for the present investigations.

Table 2. Mesh sensitivity analysis.

Serial Number	Number of Grids (Unvaned)	Relative Change in C_{PR}	Number of Grids (Vaned)	Relative Change in C_{PR}
1	103,096	-	143,550	-
2	207,480	5.92%	282,122	6.78%
3	417,606	12.00%	587,028	2.01%
4	832,944	0.32%	972,532	0.95%
5	1,680,826	1.06%	1,992,446	0.15%

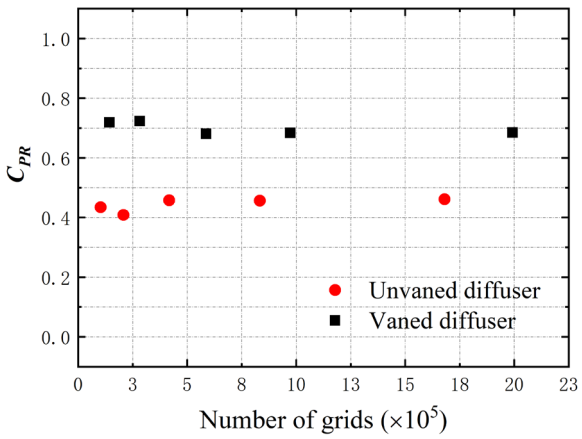

Figure 5. Grid independence test.

3. Results and Discussions

3.1. Validation of the Simulation from Diffuser Performance

Table 3 shows the comparison of pressure recovery between the steady flow simulation and Cochran & Kline measurement [7], where Equation (5) was applied to the pressure and velocity data at the mid-depth of diffuser for calculation of C_{PR}. If the uncertainty of C_{PR} being estimated between 0.012 and 0.092 in the reference [7] is considered, it may be said that C_{PR} is reasonably predicted by the present simulation. The numerical results also show that an increase of about 43% in C_{PR} is achieved after inserting a short splitter vane in the diffuser.

Table 3. Comparison of C_{PR} between simulation and experiment.

	C_{PR}: Simulation	C_{PR}: Experiment	Error (%)
Unvaned diffuser	0.456	0.437	4.35
Vaned diffuser	0.653	0.623	4.82

Distributions of pressure in the cross-sections of diffuser inlet (or throat) and the exit are displayed as pressure contours in Figure 6, where the dash-dot line shows the mid-depth. It is seen that the flow characteristics in the mid-depth section may be treatable as the flow in a two-dimensional diffuser since the pressure patterns in the transverse direction (i.e., the horizontal direction in the figure) are not much different in the vicinity of mid-depth.

Figure 7 shows the velocity field in the unvaned diffuser. It is seen that flow detachment occurs about 27.5 mm downstream of the throat on one diverging wall (i.e., the lower wall in the present case), and the main through-flow shifts toward the other diverging wall (i.e., upper wall), where no separation is observed. Note that the location of the detachment point [30] was determined by using the limiting streamline method. According to the reference [7], flow characteristics of a wide-angle of 28° of the two-dimensional diffuser are explained as follows: The flow was relatively steady, and the overall separation that was nearly two-dimensional in form extended to within a small distance from the throat on one diverging wall. In fact, these are observed in Figure 7.

Consequently, the mid-depth section of the diffuser was chosen for further analyses of computational data.

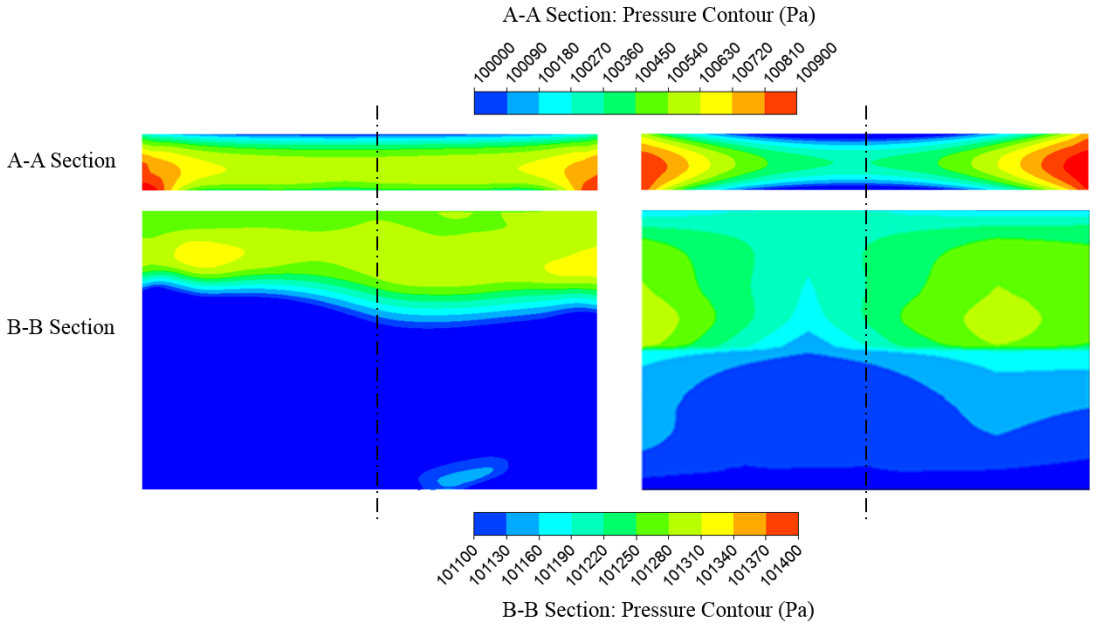

(**a**) Unvaned diffuser (**b**) Vaned diffuser

Figure 6. Pressure contours in the cross-section viewed in the downstream direction. (A-A section: diffuser throat, B-B section: diffuser exit).

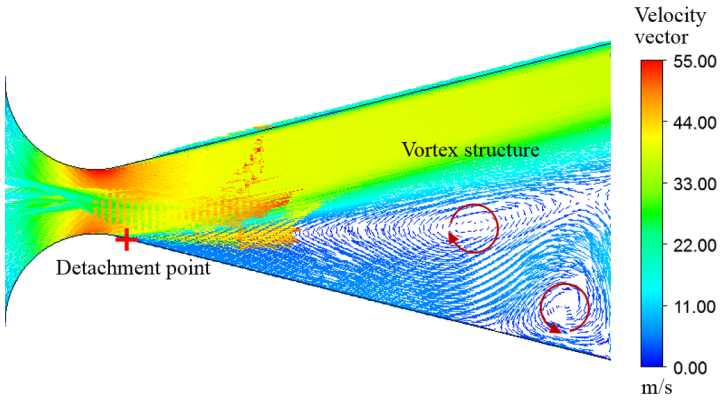

Figure 7. Velocity field in the unvaned diffuser (steady flow simulation).

3.2. Flow Characteristics

A red curve in Figure 8 shows the variation of instantaneous pressure-recovery C_{PR} with time in the case of the vaned diffuser. Though the pressure-recovery of the diffuser is really improved, flow steadiness is deteriorated. This may be because one splitter vane cannot fully eliminate the stall zone in the present diffuser. As shown in Figure 9, the fundamental frequency of C_{PR} variation is around 6.1Hz from FFT (Fast Fourier Transform) analysis. In reference [7], it is described that pulsating flow was observed due to the installation of a short vane, but there was no reliable information on its frequency and amplitude. Keeping this in mind, we examined the periodic variation of detachment-point location, the distance of which is X_S measured from the diffuser throat along the wall, and added it in Figure 8. Understandable are those features that oscillations of C_{PR} and X_S are almost in-phase, and the minimum C_{PR} appears a little bit later than the minimum X_S appears. The occurrence of the time lag may be related to the main flow inertia.

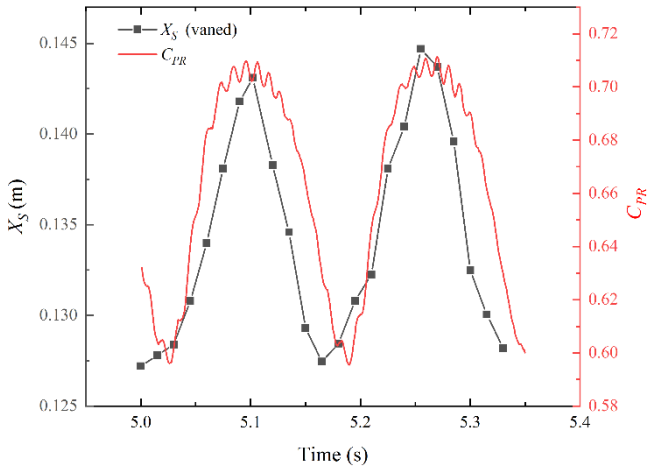

Figure 8. Variation of C_{PR} and X_S with time (vaned diffuser).

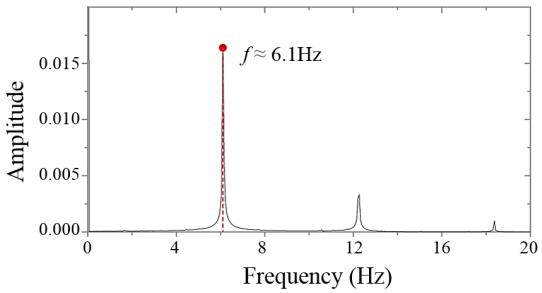

Figure 9. Fast Fourier Transform (FFT) analysis of C_{PR} (vaned diffuser).

Figure 10 shows six snapshots of the velocity field in the vaned diffuser during one time period T (=0.164 s) of flow oscillation. It is seen that the oscillatory flow is primarily related to the behaviors of the detachment point, and the stall zone extended downstream of the diffuser exit. This phenomenon occurs because one short vane cannot fully suppress the flow separation in the diffuser so that incoming main-flow tends toward the upper wall all the time. Due to this flow condition, the angle of incidence may be larger than the stall angle of a flat vane, and large-scale wake flow from the vane is always observed in the main through-flow, but it doesn't directly contact the boundary layer on the upper diverging wall.

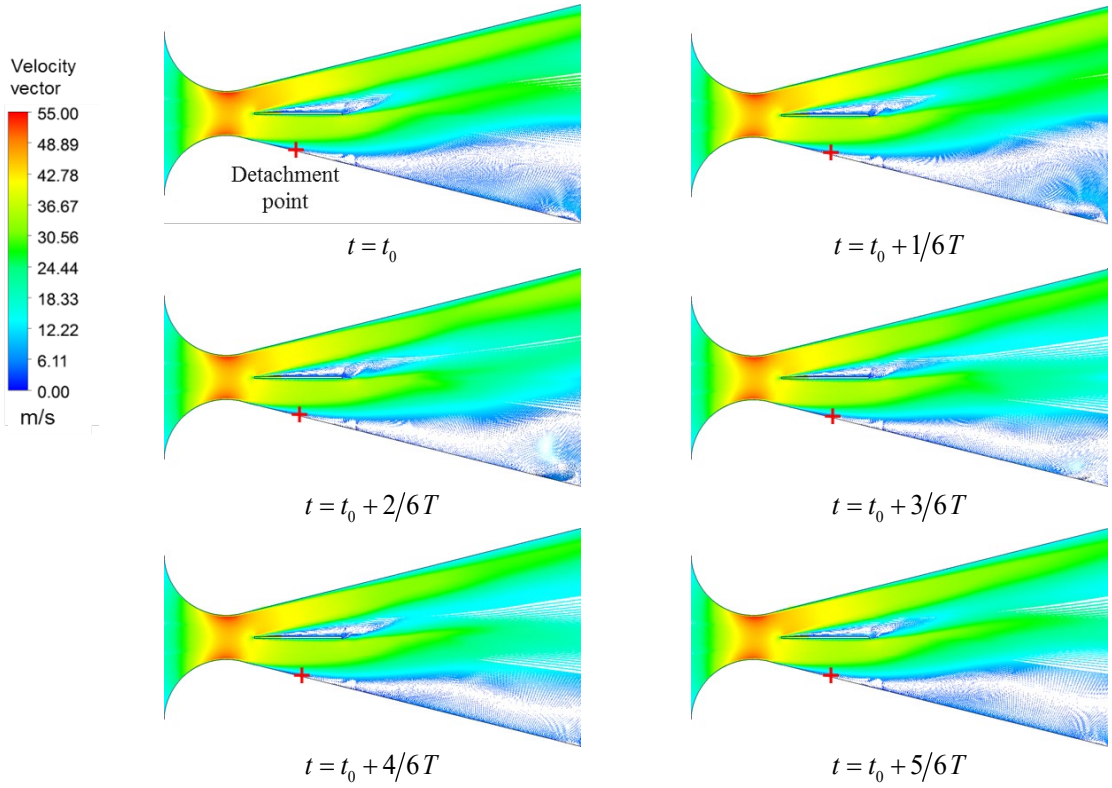

Figure 10. Snapshots of the velocity field in the vaned diffuser (t_0 = 5 s).

To see the pressure rise along the diverging wall, the following dimensionless wall-pressure p_w* is introduced:

$$p_w^* = \frac{p_w - p_{atm}}{\frac{\rho}{2}\overline{V}_1^{\,2}} \tag{6}$$

where p_w and p_{atm} denote local wall-pressure and atmospheric pressure. And $\bar{V}_1$ is the mean velocity at the throat.

By using Equation (6), six wall-pressure distributions along both upper and lower walls are obtained corresponding to the velocity fields given in Figure 11. From the results shown in Figure 11, where the right end of each p_w* curve corresponds to the diffuser exit, the following features are observed:

- As atmospheric pressure is given at the domain outlet, dimensionless wall-pressure generally decreases toward diffuser inlet from the diffuser exit.
- Since the separation of flow is observed on the lower wall and no separation on the upper wall, recovery of wall-pressure along the upper wall is greater than that along the lower wall.
- The steep adverse pressure gradient is observed in the region between the throat and location of the vane's leading-edge.
- Depending on the location of the detachment point, the shape of p_w* curve varies to some extent.

Time-averaged pressure distributions being derived during a cycle of flow oscillation are shown in Figure 12a for the vaned diffuser and Figure 12b for the unvaned diffuser. In Figure 12a, p_w* curves calculated from the steady flow simulation are drawn for comparison. The following features are found from the figures:

- In the vaned diffuser case, time-averaged p_w* curves are almost reproduced by the curves calculated from the steady flow simulation.
- In the case of the unvaned diffuser, the detachment point occurs much closer to the throat than that of the vaned case, and amounts of wall-pressure recovery reduce greatly.
- As large stall zone occupies in the unvaned diffuser, pressure rise downstream of the detachment point is almost suppressed along the lower wall.

It is noted that p_w* curves for unvaned diffuser calculated from the steady flow simulation almost coincide with those of unsteady flow simulation, as the internal flow is fairly steady in the 28° two-dimensional diffuser having area-ratio of 4.9 [7].

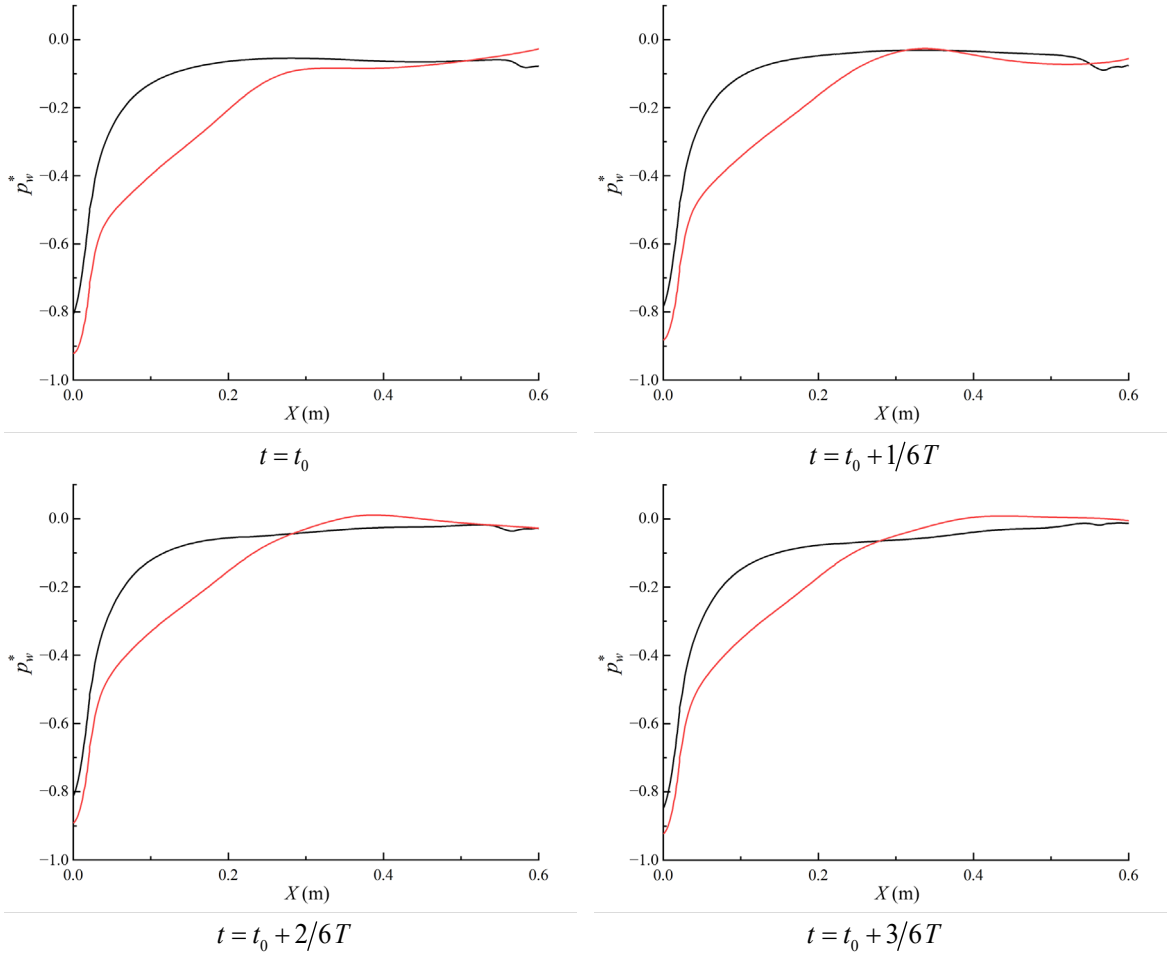

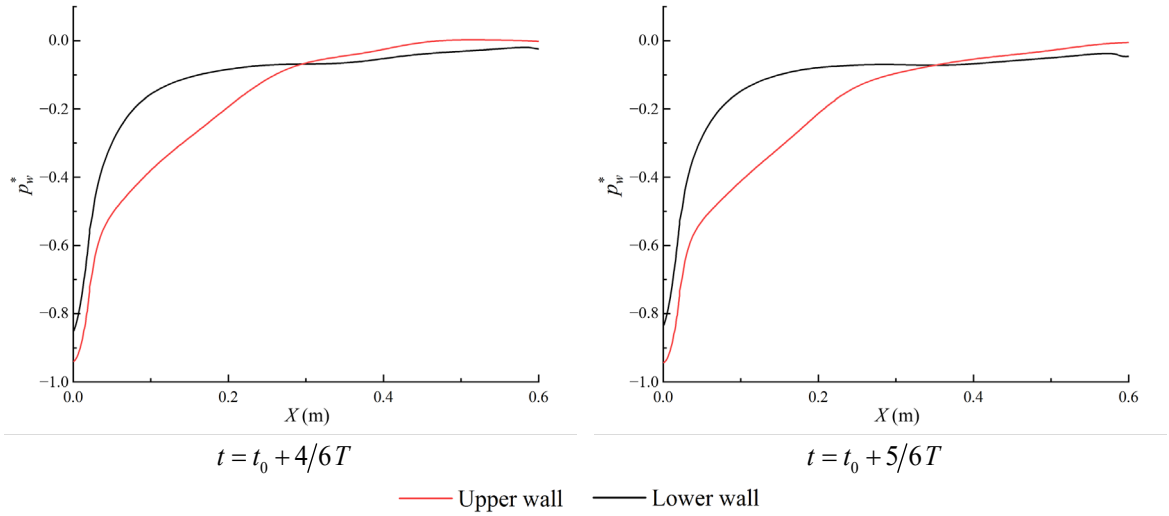

Figure 11. Distributions of wall pressure along diverging walls of the vaned diffuser.

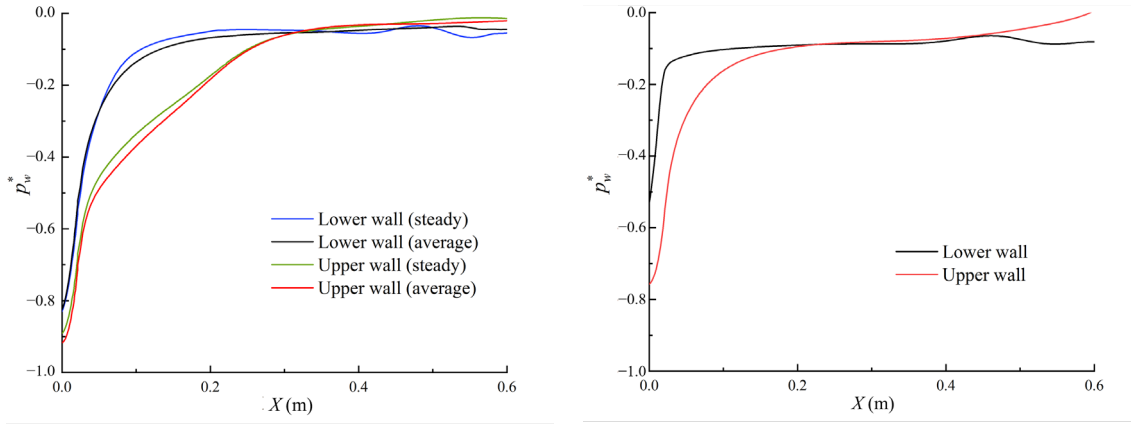

(**a**) Vaned diffuser (**b**) Unvaned diffuser

Figure 12. Time-averaged wall-pressure distributions.

3.3. Force on the Vane

The near-wall velocity-distributions on upper and lower walls at the throat section are shown in Figure 13, where Y is the distance from the center axis of the diffuser. The effects of a splitter vane are clearly observed in the boundary layer of the lower wall. That is, the boundary layer thickness decreases, and the main–flow velocity increases by inserting the vane.

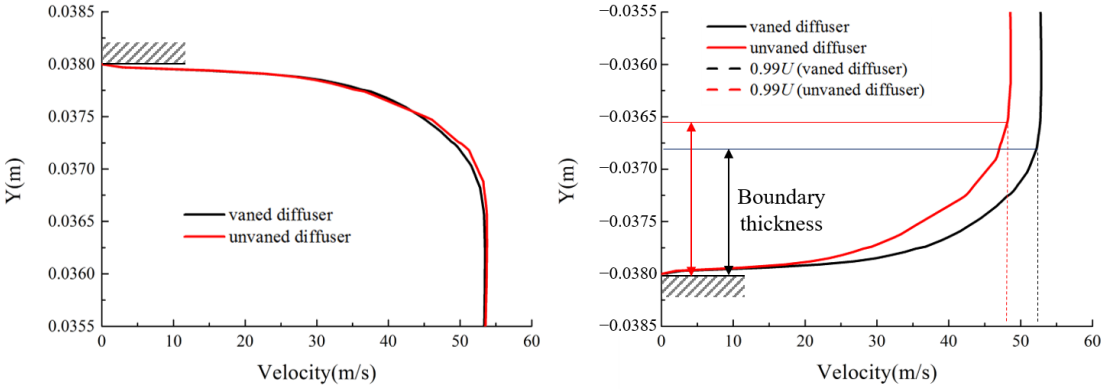

(**a**) Upper wall (**b**) Lower wall

Figure 13. Velocity distributions in the boundary layer at the throat.

To investigate the force acting on the vane in a two-dimensional diffuser, the following equation is used to calculate the dimensionless lift F_L^* assuming that the lift force is approximated by the pressure-force normal to the vane.

$$F_L^* = \frac{F_L}{\frac{\rho}{2}\overline{V}_1^{\,2} L_v} \tag{7}$$

where L_v denotes the length of splitter vane. Lift force F_L directing toward the upper wall is set as positive.

In fact, the positive value of lift force was always calculated from instantaneous pressures on the vane. After processing those data by using Equation (7), the variation of dimensionless lift with time is correlated in Figure 14, where fluctuation of detachment-point location X_S is also plotted for comparison. It is seen that the dimensionless lift oscillates between $F_L^* = 0.15$ and $F_L^* = 0.25$, having the same fundamental frequency as the pressure recovery and the location of the detachment point. Unlike the pressure-recovery (see Figure 8), the anti-phase character is observed between the location of detachment point X_S and the dimensionless lift F_L^*. The smaller X_S is, the larger F_L^* becomes, and the larger X_S is, the smaller F_L^* becomes. If the lift force acts on a vane in the flow, the reaction force of the vane pushes the flow. Thus, a so-called self-controlling mechanism is recognized in Figure 14, though the flow separation on the lower wall cannot fully be suppressed in the test case. This numerical result may quantitatively verify the qualitative explanation for the role of a splitter vane made by Senoo & Nishi [26].

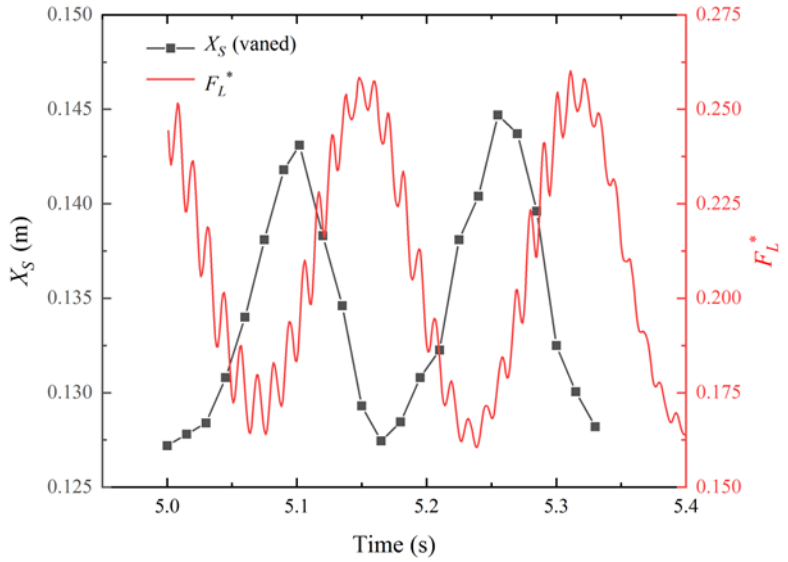

Figure 14. Lift force acting on a splitter vane.

3.4. Analysis of Unsteady Local Loss

A local energy analysis method from reference [31] was used to investigate the relationship between the flow patterns and the loss in diffusers [32]. The loss in the diffuser P_L is expressed as follows:

$$P_L = \iiint_V \frac{\partial}{\partial t}\left(\frac{1}{2}\rho\overline{u}^2\right)dV - \iiint_V \frac{\partial(-\overline{u_i}\,\overline{\rho u_i' u_j'})}{\partial x_j}dV - \iiint_V \mu\frac{\partial(\overline{u_i}\,\overline{D_{ij}})}{\partial x_j}dV + \iiint_V (-\overline{\rho u_i' u_j'})\frac{\partial \overline{u_i}}{\partial x_j}dV + \iiint_V \mu\overline{D_{ij}}\frac{\partial \overline{u_i}}{\partial x_j}dV \quad (8)$$

Term I *Term II* *Term III* *Term IV* *Term V*

where μ is the kinematic viscosity and $D_{ij} = \frac{\partial u_i}{\partial x_j} + \frac{\partial u_j}{\partial x_i}$. If a denotes a physical quantity, $\overline{a}$ and a' show the time-averaged value and the fluctuation respectively. Among the five terms, *Term I* represents the variation of the kinetic energy of the mean flow. *Term II* and *Term III* correspond to the diffusion of mean kinetic energy acting by Reynolds stress and viscous stress. *Term IV* is the turbulent kinetic energy production. And *Term V* contributes to the loss by viscous dissipation of the mean kinetic energy.

As SST *k-ω* turbulence model (RANS) was used in this study, Reynolds stress $\overline{\rho u_i' u_j'}$ was calculated as follows:

$$\overline{\rho u_i' u_j'} = -\frac{1}{2}\mu_t\left(\frac{\partial \overline{u_i}}{\partial x_j} + \frac{\partial \overline{u_j}}{\partial x_i}\right) + \frac{2}{3}\rho k\delta_{ij} \quad (9)$$

$$\delta_{ij} = \begin{bmatrix} 1 & 0 & 0 \\ 0 & 1 & 0 \\ 0 & 0 & 1 \end{bmatrix} \quad (10)$$

where μ_t, k and δ_{ij} are the eddy viscosity, the turbulent kinetic energy, and the Kronecker delta respectively.

The local loss analysis method was applied to see the contribution of each term to the loss in the diffusers. Figure 15 illustrates the terms of loss in unvaned and vaned diffusers separately (Note: λ is the loss factor that is the ratio of each term to the total loss of the mid-depth section in the unvaned diffuser). As the total loss in the vaned diffuser is around 65% of the vaned diffuser loss, the internal flow may be improved by inserting the splitter vane. The results also show that the turbulent kinetic energy production is predominant and it is the primary component of the loss for both diffusers.

Considering that the total loss in the present diffuser is mostly caused by the turbulent kinetic energy production, visualization of its distribution in the vaned diffuser was conducted to see the effect of vane installation. Figure 16 shows such six pictures corresponding to the time used in Figure 10, where the velocity fields are displayed. There are two apparent zones that correspond to the shear layer, where the amount of turbulent kinetic energy production is large. One is observed at the boundary between the main flow and the detached boundary-layer flow (or stall zone) on the lower wall of the diffuser. The other appears in the mixing layer between the main flow and the separating flow from the vane surface (i.e., suction side) faced the upper wall. And it is seen that the highest production occurs in the boundary caused by the leading-edge separation of the vane.

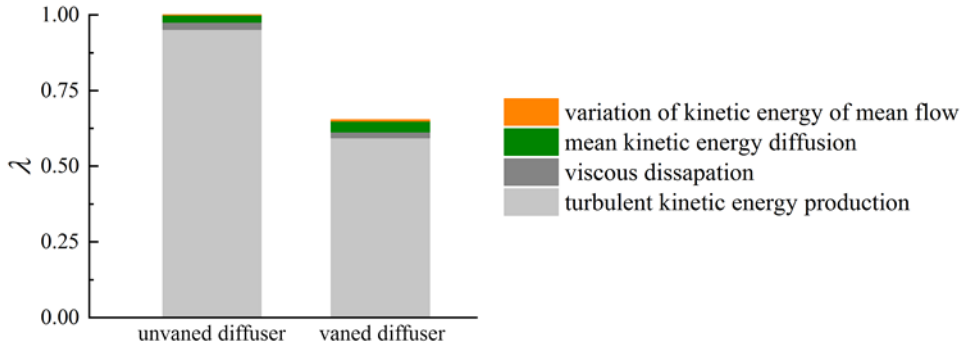

Figure 15. Composition of diffuser loss predicted in unvaned and vaned diffusers.

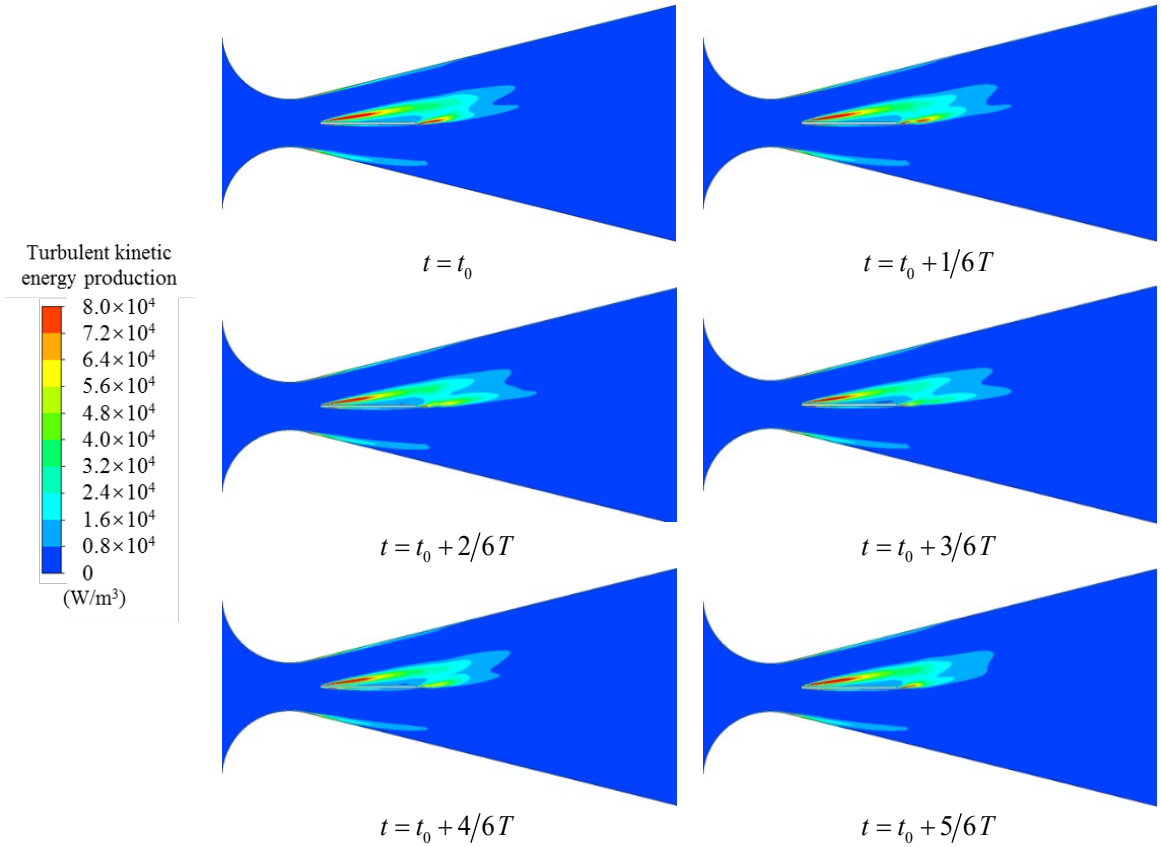

Figure 16. Distributions of turbulent kinetic energy production in vaned diffuser.

4. Concluding Remarks

From the numerical simulation of incompressible flow in a wide-angle of 28° two-dimensional diffuser with and without a short splitter vane, the following concluding remarks are drawn:

1. Improvement of pressure-recovery by the vane and oscillatory diffuser-flow reported in the experimental study done by Cochran & Kline (1958) are reasonably simulated.

2. The unsteady flow simulation shows that the lift force acting on the vane varies periodically in the opposite phase with the detachment point moved back and forth on a diverging wall since one vane is not sufficient to fully suppress the flow separation and the incoming main-flow shifts toward the other diverging wall in the diffuser.

3. As a role of splitter vane in the diffuser, "the lift force of the vane is a key factor" may be verified quantitatively from the present numerical simulation.

4. The local loss analysis shows that the turbulent kinetic energy production observed in mixing layers contributes most of the loss in the diffuser.

5. Distributions of time-averaged velocity and wall-pressure calculated from unsteady flow simulation are reproduced from steady flow simulation reasonably.

6. Consequently, the present numerical technique may be usable to investigate the flow character in a wide-angle diffuser with splitter vanes at a design stage.

Author Contributions: Investigation, X.M.; data curation, X.M.; writing—original draft preparation, X.M.; writing—review and editing, Z.Z., M.N., and S.L.; visualization, M.X., M.N., and S.L.; supervision, Z.Z., M.N., and S.L. All authors have read and agreed to the published version of the manuscript.

Funding: This research was funded by National Key R&D Program of China (2018YFB0606101) and National Natural Science Foundation of China (No.51876100)

Conflicts of Interest: The authors declare that they have no conflict of interest.

References

1. Liu, S.; Wu, Y.; Chen, T.; Nishi, M. Development of Numerical Performance Test Stand for a Kaplan Turbine. *Int. J. Turbo Jet-Engines* **2009**, *24*, 253–262.
2. Guénette, V.; Houde, S.; Ciocan, G.D.; Dumas, G.; Huang, J.; Deschênes, C. Numerical Prediction of a Bulb Turbine Performance Hill Chart through RANS simulations. In Proceedings of the 26th IAHR Symposium on Hydraulic Machinery and Systems, Beijing, China, 19–23 September 2012.
3. Ruopp, A.; Ruprecht, A.; Riedelbauch, S.; Arnaud, G.; Hamad, I. Development of a Hydro Kinetic River Turbine with Simulation and Operational Measurement Results in Comparison. In Proceedings of the 27th IAHR Symposium on Hydraulic Machinery and Systems, Montreal, QC, Canada, 22–26 September 2014.
4. Eckert, W.T.; Mort, K.W.; Jope, J. *Aerodynamic Design Guidelines and Computer Program for Estimation of Subsonic Wind Tunnel Performance*; NASA-TN-D-8243; NASA Ames Research Center: Moffett Field, CA, USA, 1976.
5. King, C.D.; Ölçmen, S.M.; Sharif, M.A.R.; Presdorf, T. Computational Analysis of Diffuser Performance for Subsonic Aerodynamic Research Laboratory Wind Tunnel. *Eng. Appl. Comput. Fluid Mech.* **2013**, *7*, 419–432.
6. Vassiliev, V.; Irmisch, S.; Florjancic, S. CFD Analysis of Industrial Gas Turbine Exhaust Diffusers. In Proceedings of the ASME TURBO EXPO2002, Amsterdam, The Netherlands, 3–6 June 2002
7. Cochran, D.L.; Kline, S.J. *The Use of Short Flat Vanes for Producing Efficient Wide-Angle Two-Dimensional Subsonic Diffusers*; NACA-TN-4309; National Advisory Committee for Aeronautics: Washington, DC, USA, 1958.
8. Moore, C.A., Jr.; Kline, S.J. *Some Effects of Vanes and of Turbulence in Two-Dimensional Wide-Angle Subsonic Diffusers*; NACA-TN-4080; National Advisory Committee for Aeronautics: Washington, DC, USA, 1958.
9. Reneau, L.R.; Johnston, J.P.; Kline, S.J. Performance and Design of Straight, Two-dimensional Diffusers. *ASME Trans. J. Basic Eng.* **1967**, *89*, 141–150.
10. Cockrell, D.J.; Markland, E. A Review of Incompressible Diffuser Flow. *Aircr. Eng. Aerosp. Technol.* **1963**, *35*, 286–292.
11. Sovran, G.; Klomp, E.D. Experimentally Determined Optimum Geometries for Rectilinear Diffusers with Rectangular, Conical or Annular Cross-Section. In *Fluid Mechanics of Internal Flow*, Proceedings of the symposium on the fluid mechanics of internal flow, Warren, MI, USA, 1965; Elsevier: New York, USA, 1967; 270-312.
12. Furuya, Y.; Fujimoto, T.; Yamazato, E.; Tsuzuki, I.; Nishiura, I. Performance of the Two-Dimensional Diffusers with Suction at the Entrance. *Bull. JSME* **1970**, *13*, 264–271.

13. Nicoll, W.B.; Ramaprian, B.R. Performance of Conical Diffusers with Annular Injection at Inlet. *ASME Trans. J. Basic Eng.* **1970**, *92*, 827–835.
14. Hoffmann, J.A. Effects of Free-stream Turbulence on Diffuser Performance. *ASME Trans. J. Fluids Eng.* **1981**, *103*, 385–390.
15. Senoo, Y.; Nishi, M. Improvement of the Performance of Conical Diffusers by Vortex Generators. *ASME Trans. J. Fluids Eng.* **1974**, *96*, 4–10.
16. Reichert, B.A.; Wendt, B. J Improving Curved Subsonic Diffuser Performance with Vortex Generators. *AIAA J.* **1996**, *34*, 65–72.
17. Nishi, M.; Yoshida, K.; Morimitsu, K. Control of Separation in a Conical Diffuser by Vortex Generator Jets. *JSME Int. J. Ser. B Fluids Therm. Eng.* **1998**, *41*, 233–238.
18. Feil, O.G. Vane Systems for Very-wide-angle Subsonic Diffusers. *ASME Trans. J. Basic Eng.* **1964**, *86*, 759–764.
19. Majumdar, B.; Singh, S.N.; Agrawal, D.P. Flow Characteristics in a Large Area Ratio Curved Diffuser. *Proc. Inst. Mech. Eng. Part G J. Aerosp. Eng.* **1996**, *210*, 65–75.
20. Chong, T.P.; Joseph, P.F.; Davies, P.O.A.L. Design and Performance of an Open Jet Wind Tunnel for Aero-Acoustic Measurement. *Appl. Acoust.* **2009**, *70*, 605–614.
21. Chiekh, M.B.; Béra, J.-C.; Sunyach, M. Synthetic Jet Control for Flows in a Diffuser: Vectoring, Spreading and Mixing Enhancement. *J. Turbul.* **2003**, *4*, 37–41
22. Sun, C.L.; Lin, G.C. The Flow Rectification of a Vaned Micro diffuser: A Numerical Investigation. *J. Chin. Inst. Eng.* **2010**, *33*, 1–13.
23. Ghose, S.; Kline, S.J. The Computation of Optimum Pressure Recovery in Two-Dimensional Diffusers. *ASME J. Fluids Eng.* **1978**, *100*, 419–426.
24. Bardina, J.; Lyrio, A.; Kline, S.J.; Ferziger, J.H.; Johnston, J.P. A Prediction Method for Planar Diffuser Flows. *ASME J. Fluids Eng.* **1981**, *103*, 315–321.
25. Kline, S.J. On the Nature of Stall. *ASME Trans. J. Basic Eng.* **1959**, *81*, 305–320.
26. Senoo, Y.; Nishi, M. Prediction of Flow Separation in a Diffuser by a Boundary Layer Calculation. *ASME Trans. J. Fluids Eng.* **1977**, *99*, 379–389.
27. Menter, F.R.; Kuntz, M.; Langtry, R. Ten Years of Industrial Experience with the SST Turbulence Model. *Turbul. Heat Mass Transf.* **2003**, *4*, 625–632.
28. El-Behery, S.M.; Hamed, M.H. A Comparative Study of Turbulence Models Performance for Separating Flow in a Planar Asymmetric Diffuser. *Comput. Fluids* **2011**, *44*, 248–257.
29. ANSYS Help. *ANSYS Help Viewer 14.5*; SAS IP, Inc.: Cary, NC, USA, 2012.
30. Simpson, R.L. Review—A Review of Some Phenomena in Turbulent Flow Separation. *ASME Trans. J. Fluids Eng.* **1981**, *103*, 520–533.
31. Lu, G.; Zuo, Z.; Liu, D.; Liu, S. Energy Balance and Local Unsteady Loss Analysis of Flows in a Low Specific Speed Model Pump-Turbine in the Positive Slope Region on the Pump Performance Curve. *Energies* **2019**, *12*, 1829.
32. Wilhelm, S.; Balarac, G.; Métais, O.; Ségoufin, C. Analysis of Head Losses in a Turbine Draft Tube by Means of 3D Unsteady Simulations. *Flow Turbul. Combust.* **2016**, *97*, 1255–1280.